Supplementary Material for Dalton Transactions

Supplementary Information

Preparation, Electrochemical and Spectral Properties of Free-Base and Manganese *N*-methyl-Pyridylethynyl Porphyrins

Ching-Yao Lin,* Yen-Chuan Chen, Chi-Wen Yao, Sung-Chou Huang and Yi-Hui Cheng

Department of Applied Chemistry, National Chi Nan University. 302 University Road, Puli, Nantou Hsien 54561, Taiwan.

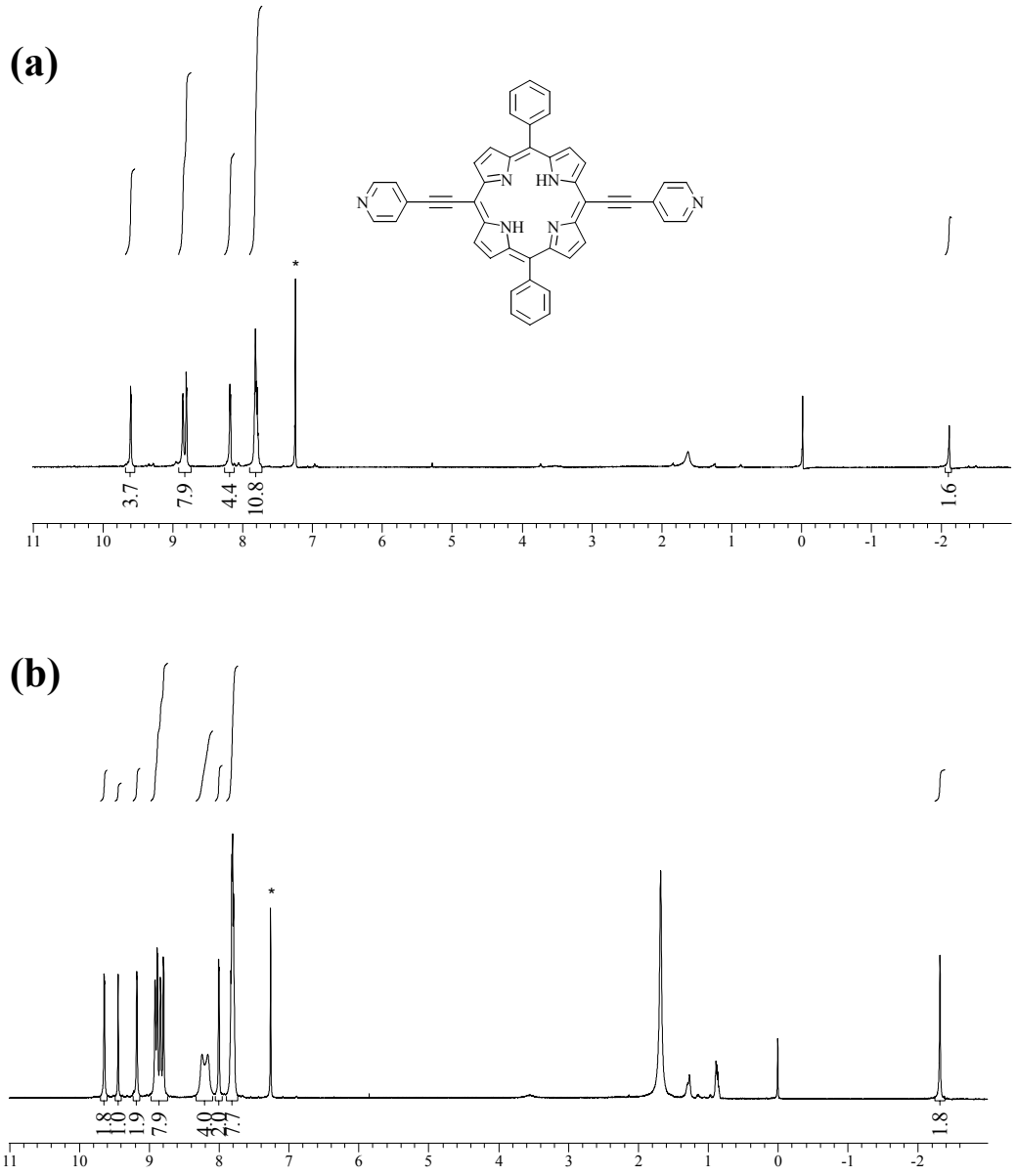

Figure 1. ^{1}H-NMR spectra of (a) un-methylated H_2 **6** precursor from Lindsey's copper-free cross-coupling method and (b) major product from de-metallation of Zn **6** precursor. Comparison of two NMR spectra shows that de-metallation of Zn **6** precursor does not yield H_2 **6** precursor as the major product.

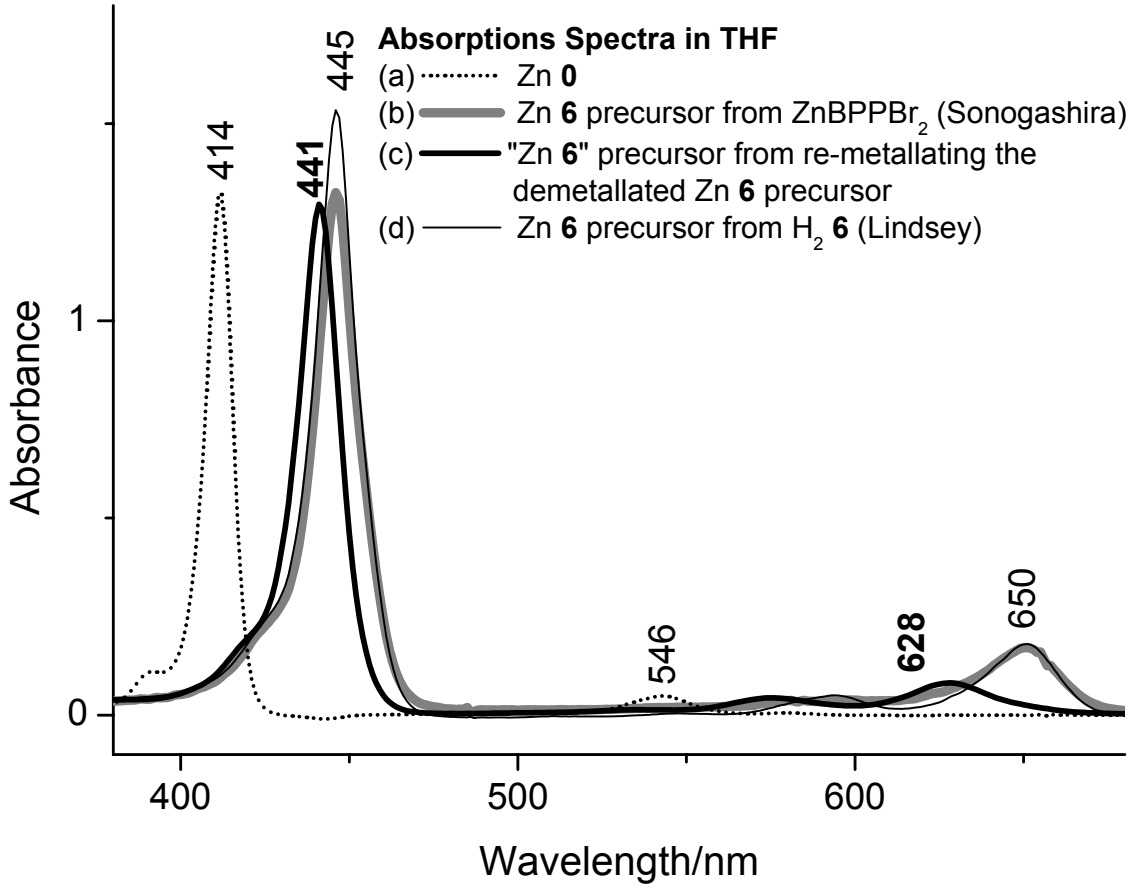

Figure 2. UV-Visible spectra of (a) ZnBPP (b) un-methylated Zn **6** precursor from Sonogashira cross-coupling reaction of $ZnBPPBr_2$ with 4-pyridylethyne (c) "Zn **6**" precursor from demetallating Zn **6** then metallating with Zn^{2+} (d) Zn **6** precursor from metallating Zn^{2+} with H_2 **6** precursor (from Lindsey's copper-free cross-coupling reaction). (c) shows that de-metallation of Zn **6** precursor does not generate H_2 **6** precursor.

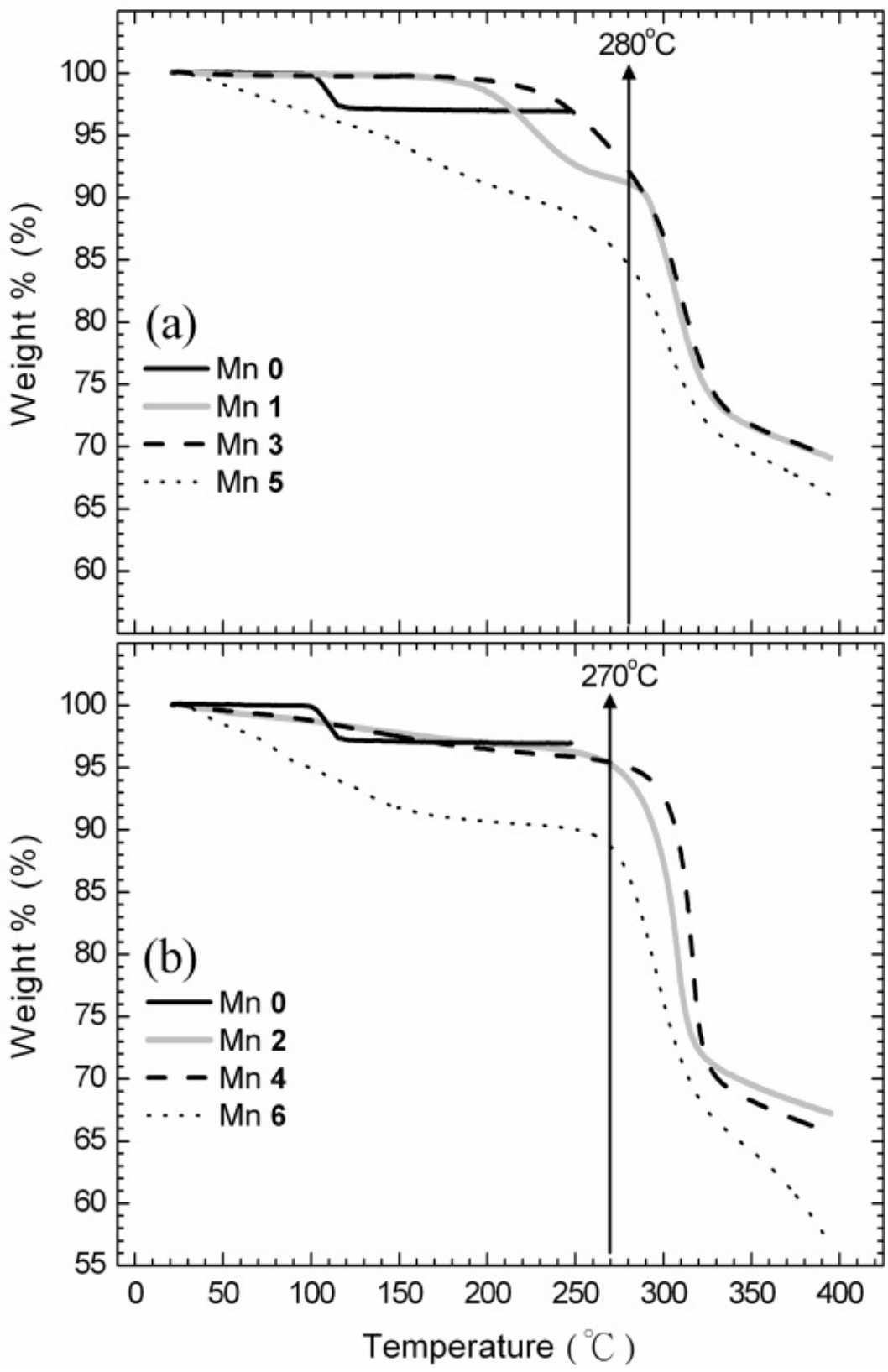

Figure 3. TGA (10°C/min) of (a) Mn **0**, Mn **1**, Mn **3**, Mn **5,** (b)Mn **0**, Mn **2**, Mn **4** and Mn **6**.

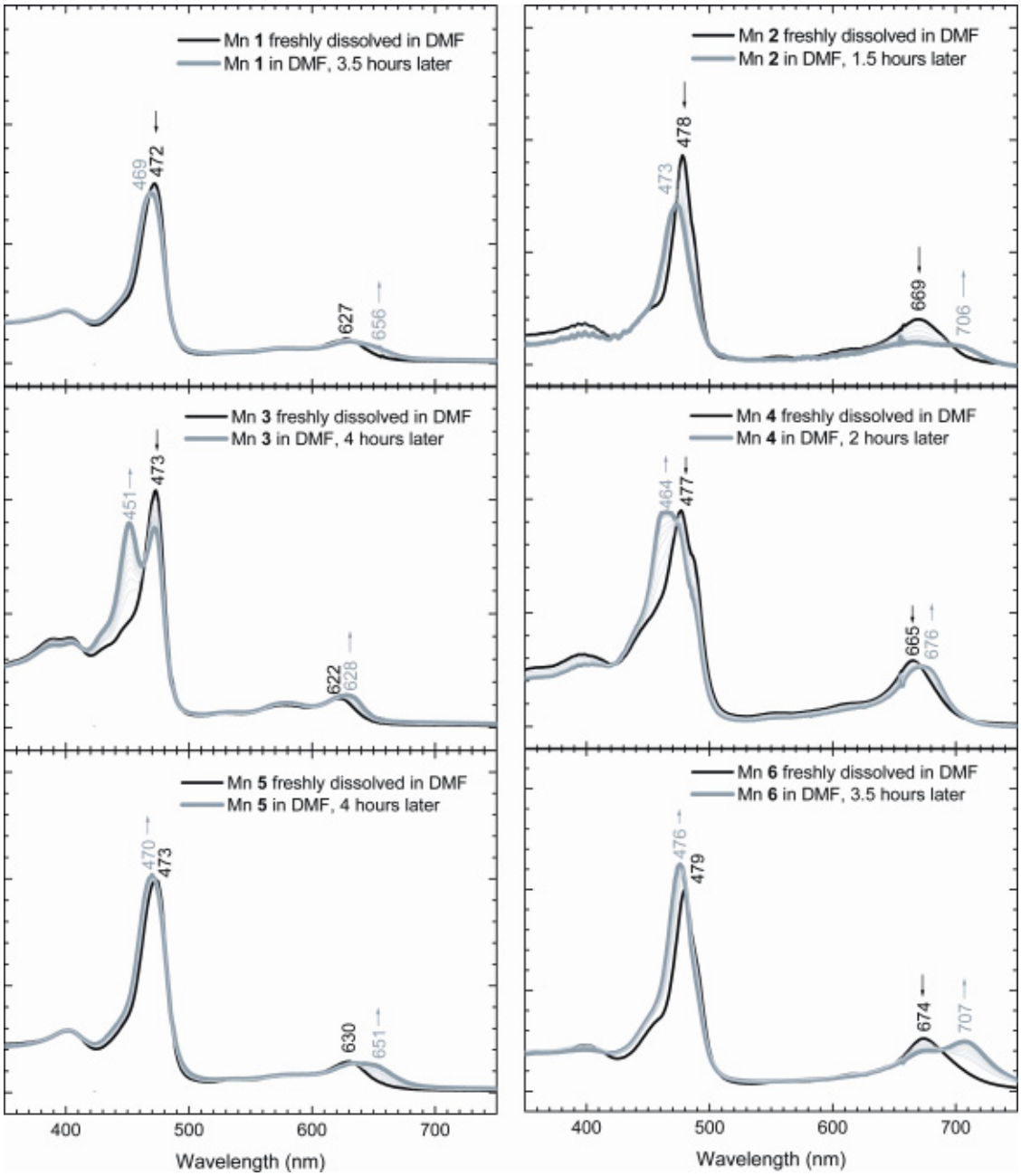

Figure 4. UV-Visible spectrum changes of Mn **0** – **6** dissolved in DMF. The spectrum changes are consistent with $Mn^{III/II}$ **0** – **6** reductions. The final spectra are mixtures of Mn^{III} and Mn^{II} **0** – **6** (grey lines).

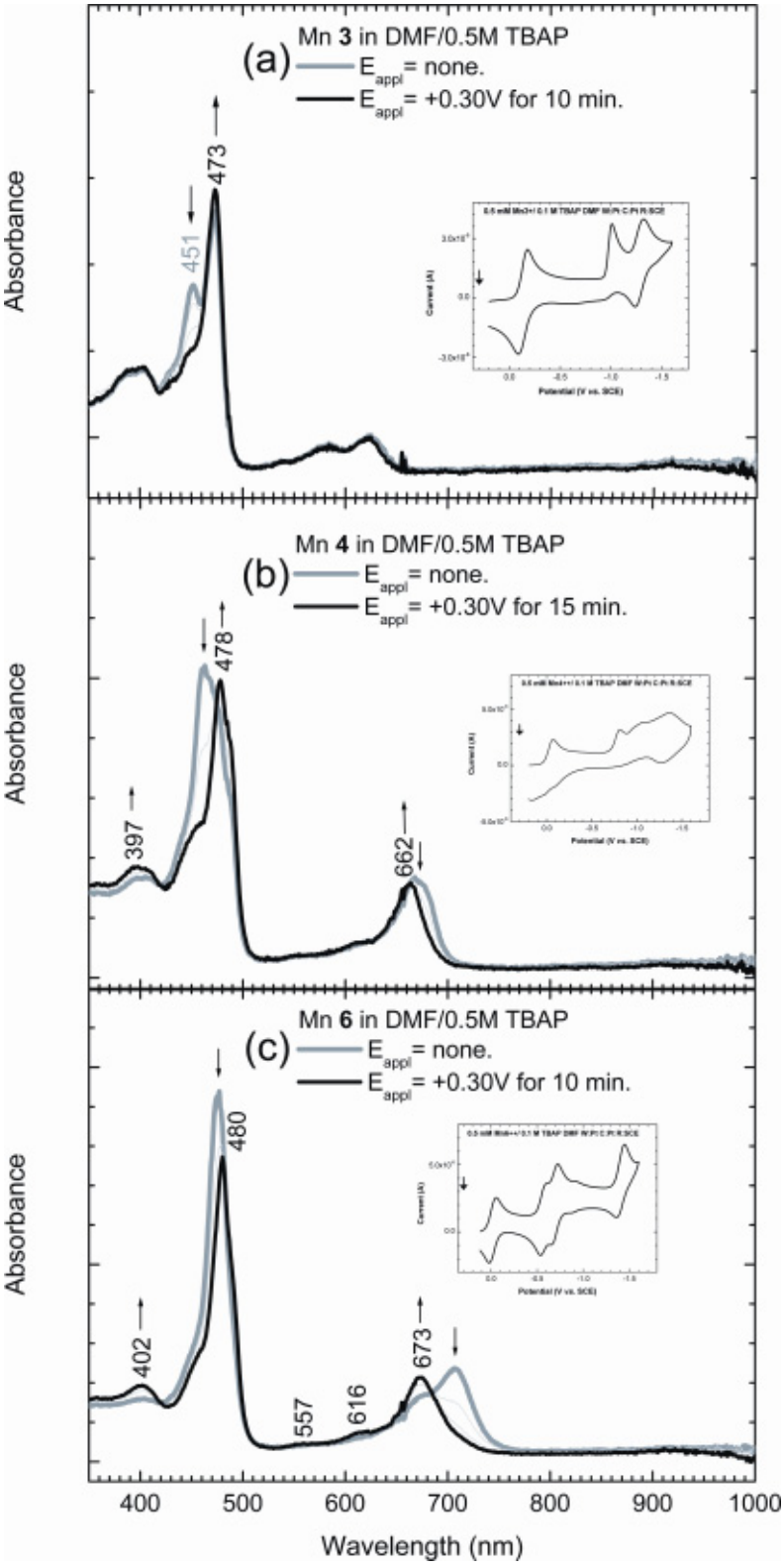

Figure 5. UV-Visible spectrum changes of $Mn^{III/II}$ **3**, **4**, and **6** mixtures upon applying +0.30 V *vs*. SCE. These spectro-electrochemical experiments verify our suggestion that Mn^{III} **0** – **6** undergo auto-reduction in DMF solutions.

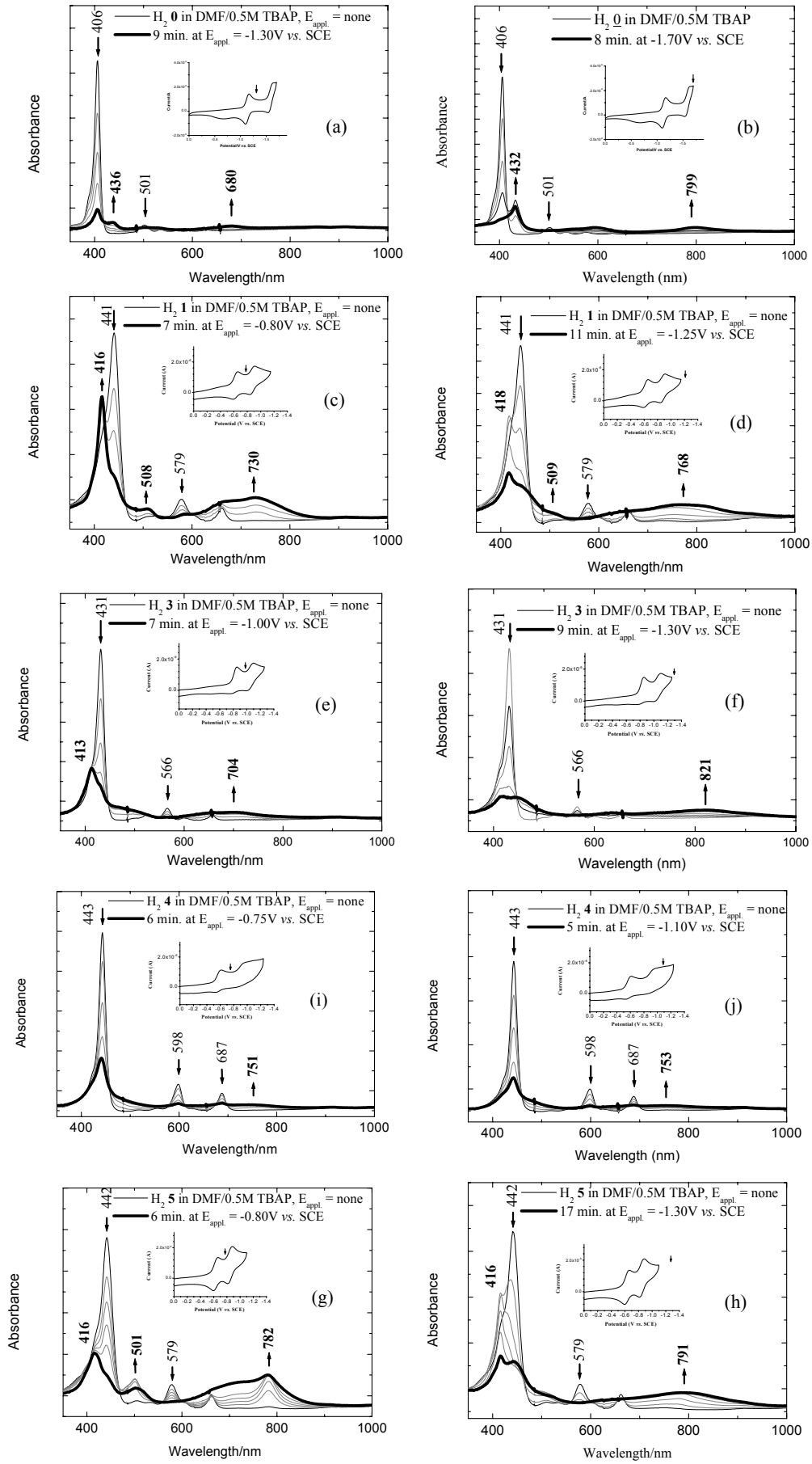

Figure 6. UV-Visible spectrum changes of H_2 **0**, **1**, **3**, **5** and **4** upon thin-layer reductions.

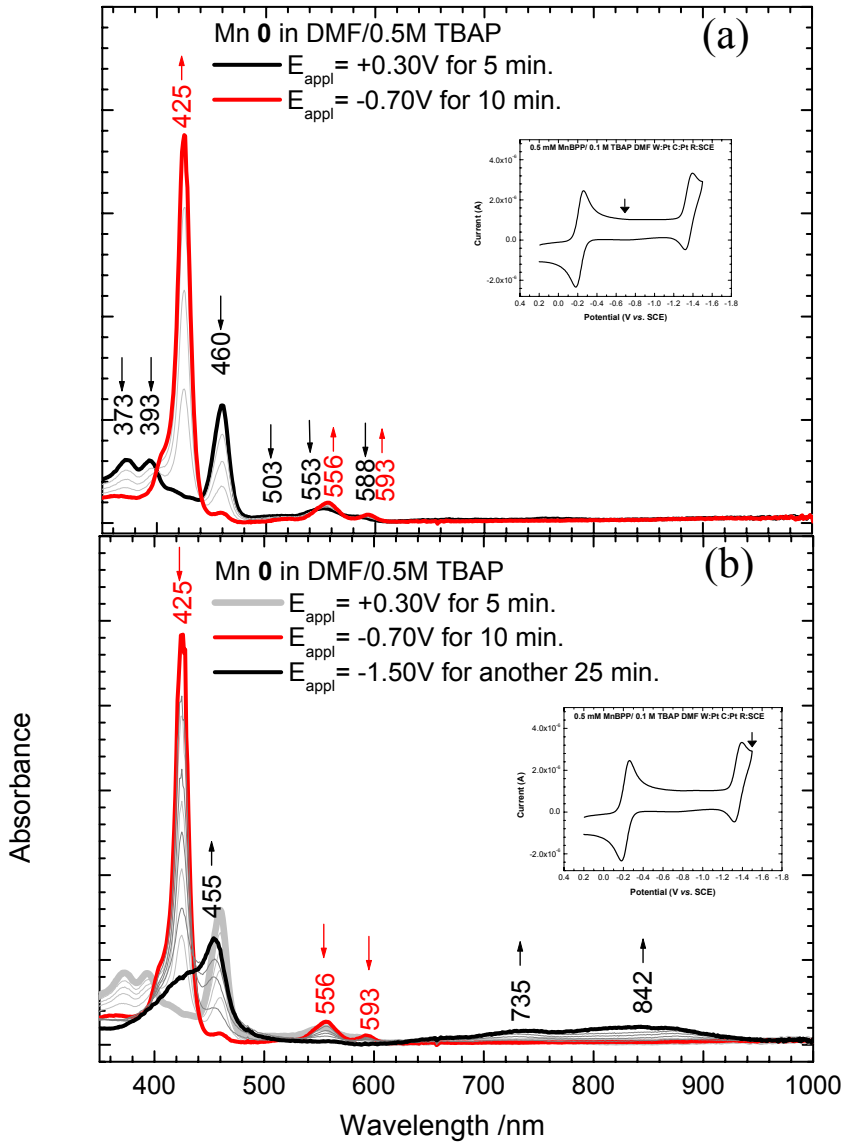

Figure 7. UV-Vis ible spectrum changes of Mn **0** upon thin-layer reductions. Recovery rates at +0.30 V *vs*. SCE (a) 99% (b) 94%.

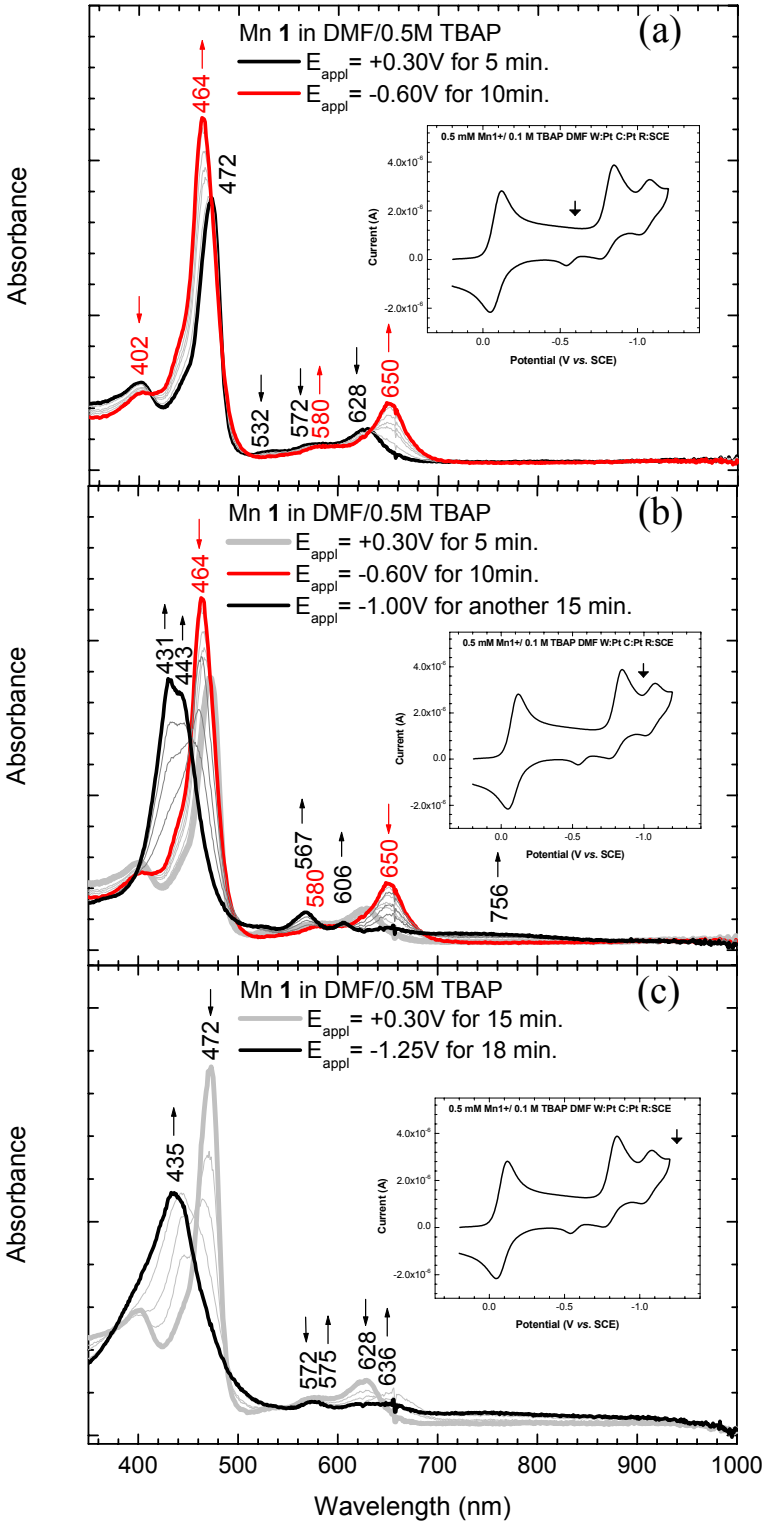

Figure 8. UV-Visible spectrum changes of Mn **1** upon thin-layer reductions. Recovery rates at +0.30 V *vs*. SCE (a) 99% (b) not reversible (c) not reversible.

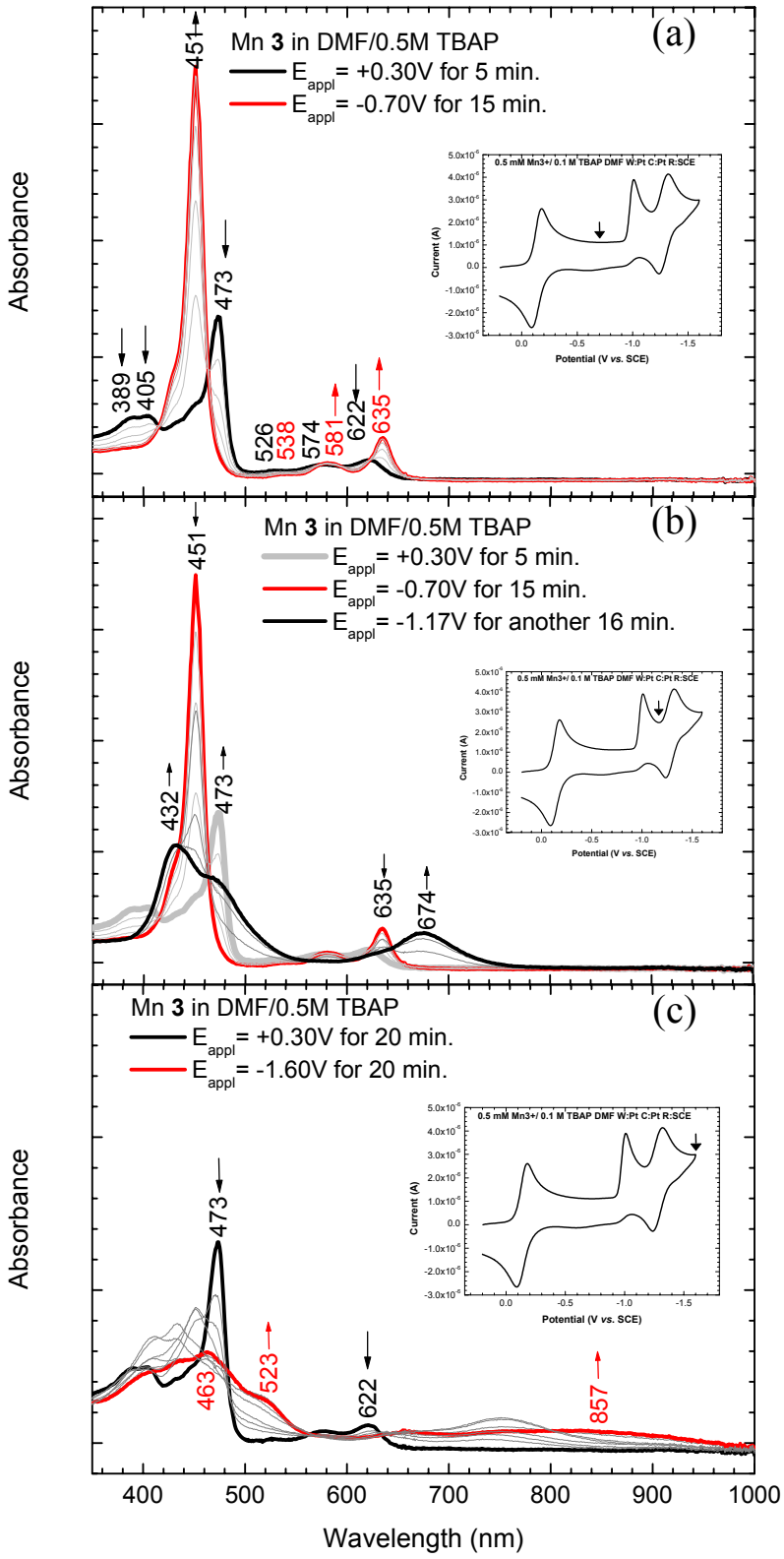

Figure 9. UV-Visible spectrum changes of Mn **3** upon thin-layer reductions. Recovery rates at +0.30 V *vs*. SCE (a) 96% (b) 99% (c) 51%.

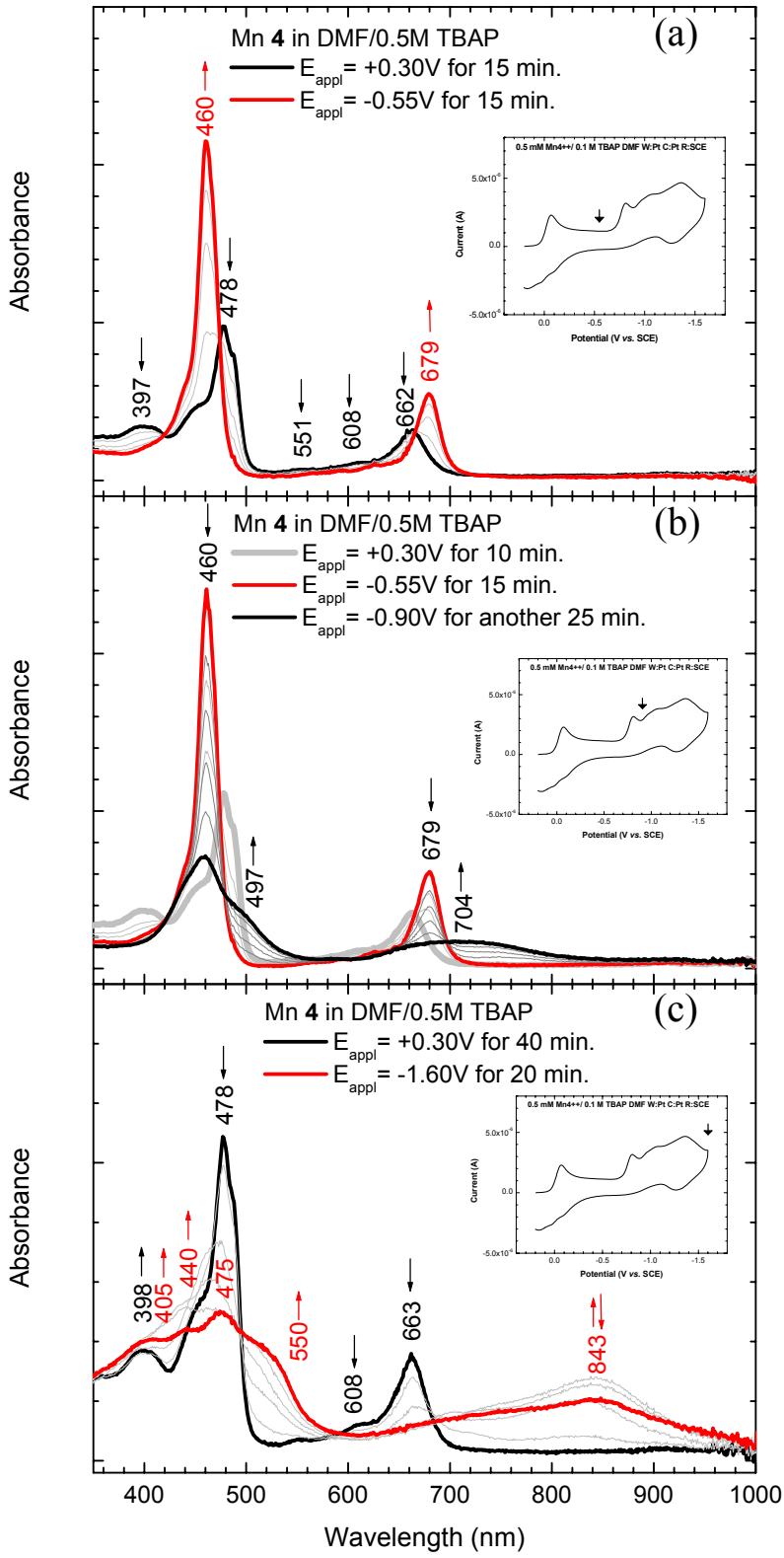

Figure 10. UV-Visible spectrum changes of Mn **4** upon thin-layer reductions. Recovery rates at +0.30 V *vs*. SCE (a) 99% (b) 83% (c) 70%.

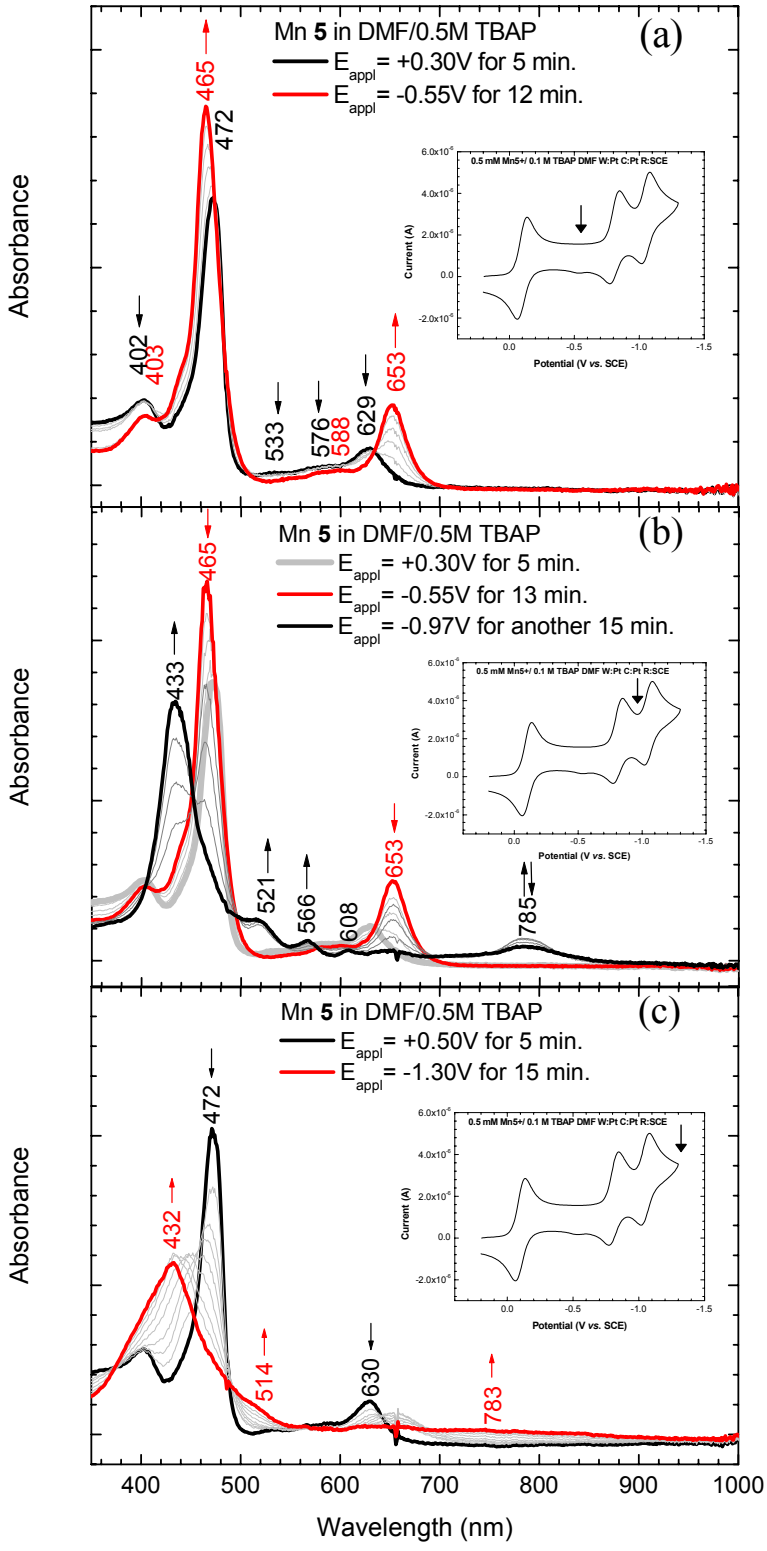

Figure 11. UV-Visible spectrum changes of Mn **5** upon thin-layer reductions. Recovery rates at +0.30 V *vs*. SCE (a) 99% (b) not reversible (c) not reversible.

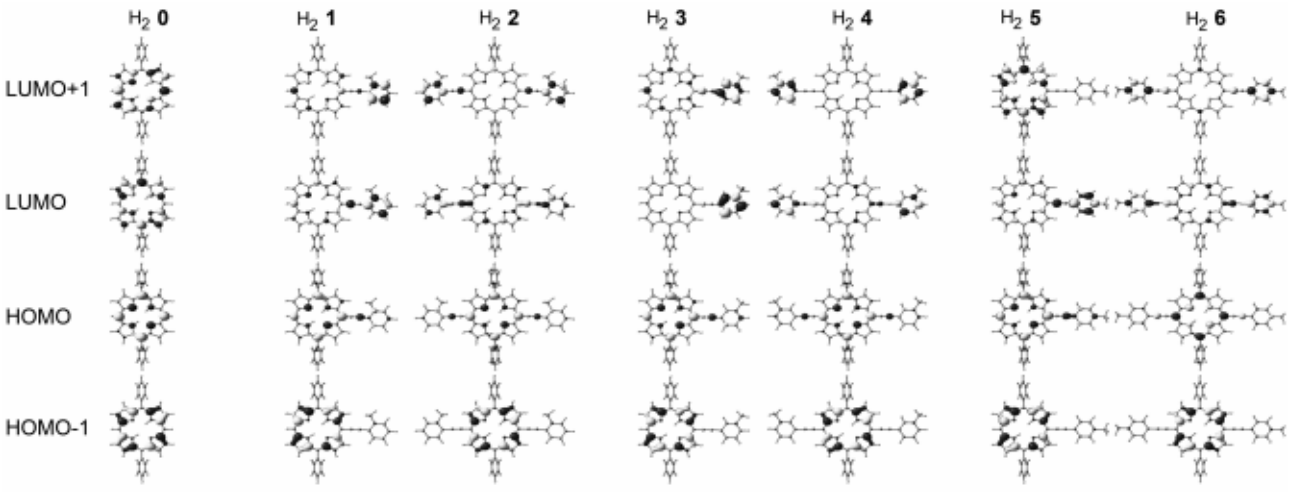

Figure 12. Calculated Frontier Molecular Orbitals of H_2 **0** to **6** (B3LYP/LanL2DZ, all IR frequencies of the optimized structures were checked to be positive). Note that these MO patterns are only used to qualitatively compare with the experimentally results.

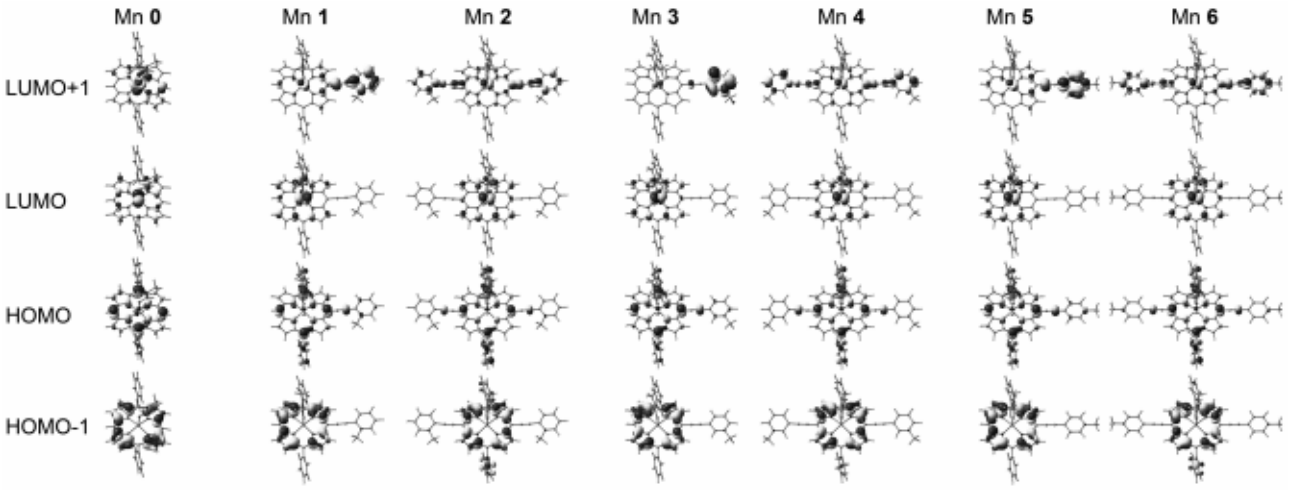

Figure 13. Calculated Frontier Molecular Orbitals of Mn **0** to **6** (B3LYP/LanL2DZ, all IR frequencies of the optimized structures were checked to be positive). Note that these MO patterns are only used to qualitatively compare with the experimentally results.